RAPID COMMUNICATIONS

PHYSICAL REVIEW B VOLUME 35, NUMBER 8 15 MARCH 1987-I

Elastic constants of Mo/Ta superlattices measured by Brillouin scattering

J. A. Bell, W. R. Bennett, R. Zanoni, G. I. Stegeman, C. M. Falco, and F. Nizzoli*
Optical Sciences Center, University of Arizona, Tucson, Arizona 85721
(Received 13 November 1986)

The elastic properties of Mo/Ta superlattices and the dependences on bilayer wavelength over the range 7–200 Å are investigated. These are the first such measurements for a bcc-bcc system, and significant differences from previously studied metal superlattices are found. Surface velocities of as many as 12 acoustic modes guided by the thin-film samples have been measured using Brillouin spectroscopy. The elastic constants c_{11}, c_{13}, c_{33}, and c_{44} for the superlattices are determined by fitting the data to an acoustic model of supported hexagonal films. We compare these stiffnesses with those predicted from the bulk constituent properties. The relative Brillouin cross section is found to be accurately represented by a pure ripple scattering theory with no photoelastic contribution.

Unexpected softening of the elastic constants of metal superlattices for several material combinations has been recently reported.[1-4] This behavior has been seen as a substantial decrease in the Rayleigh surface wave velocity for a range of superlattice bilayer wavelengths (Λ). The similarity of this effect, exhibited in differing materials, has lead to the conclusion that such a softening is a universal property in metal superlattices.[5] We note, however, that the metal combinations used in these previous studies are all bcc-fcc. In this paper, we discuss the elastic properties of Mo/Ta superlattices, which have a bcc-bcc structure.

For most metals, surface ripple is the dominant mechanism for Brillouin scattering,[6] the process by which light couples to thermal fluctuations in matter. Thermally excited acoustic phonons, which corrugate the nominally planar surface, produce a small cross section for inelastic optical scattering. The component of momentum parallel to the surface is conserved in this process and the shift in frequency of the scattered light depends on the geometry of the incident and the scattered beams and the surface acoustic phase velocity. The light-scattering measurements we have performed were sufficiently sensitive to determine the velocities of as many as 11 Sezawa waves (generalized Lamb waves[7]), which are guided by the thin film as well as the surface Rayleigh wave.

A dual-beam sputtering system with a rotating substrate platform[8] is used in preparing the samples. The substrates are fused silica and 90° single-crystal sapphire. Active control of the sputter parameters enables the deposition rate to be held constant to within $\pm 0.3\%$ throughout the growth of a sample. Rutherford backscattering, x-ray diffraction, and optical interferometry measurements have been performed to calibrate the deposition rates for each metal. Structural characterization of the samples was accomplished with standard Cu $K\alpha$ x-ray diffraction equipment. Film thicknesses of samples with Λ in the range 13–100 Å were found by measuring the angular separation of satellite peaks in scans from a θ-2θ diffractometer. These thickness measurements are in good agreement with those obtained using the calibrated sputtering rates combined with the bulk densities for the constituent metals. Two sets of samples have been studied, the first having total thicknesses of $\cong 3500$ Å and 50% molybdenum by volume, while films in the second set are $\cong 4400$ Å thick with 54% molybdenum. We find from x-ray Laue exposures that both molybdenum and tantalum grow with the (110) plane nearly parallel to the substrate surface. Read camera photographs show that the crystallites are oriented randomly and uniformly about the axis normal to the surface. The lateral coherence length is typically a few hundred angstroms[8] (small compared to the acoustic wavelengths involved). This structural information allows predictions of the elastic constants to be made based on the bulk properties of the single-crystal constituent metals.[9] The Voigt (Reuss) estimate for the polycrystalline elasticity[10] is found by analytically averaging over the stiffness (compliance) tensor for the orientational distribution for the crystallites and corresponds to an upper (lower) limit to the stiffness constants. The resulting symmetry for such an aggregate film is hexagonal, allowing direct application of a recent analysis[11] of the effective elastic constants of a superlattice composed of anisotropic media. This final step is valid for acoustic wavelengths much larger than the layer thicknesses.

Our experimental technique for detecting surface Brillouin scattering is based on recent advances in high-resolution, high-contrast spectroscopy.[12] An argon-ion laser with a single longitudinal mode at $\lambda = 5145$ Å is focused to a $\cong 20$-μm spot on the sample with the field p polarized. Effects of heating are undetected for intensities limited to 200 mW in the case of samples grown on sapphire and 50 mW for those on fused silica. Scattered light, within a circular 0.04-sr beam and centered in the saggital plane, is collected and collimated. A scanning six-pass tandem Fabry-Perot interferometer[12] is then used to frequency analyze the light. The detector is an FW130 photomultiplier tube with a dark count rate of $\cong 0.3\ \text{sec}^{-1}$. To prevent detector saturation, an acousto-optic modulator attenuates the laser by $\cong 10^{-3}$ while scanning through the bright elastically scattered light. A microcomputer is equipped to record the photon counts, drive the Fabry-Perot scan at 1 Hz and actively align both cavities to a 10-Å tolerance for periods of many hours.

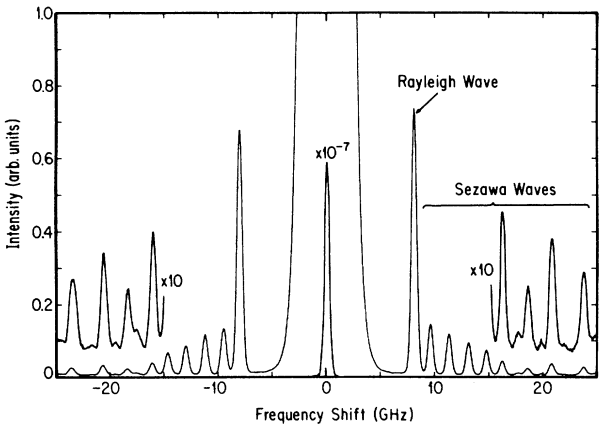

FIG. 1. Typical surface spectrum obtained from a 4480-Å-thick Mo/Ta superlattice on sapphire with bilayer wavelength of $\Lambda = 160$ Å. The unshifted peak is shown at much reduced scale to indicate the instrumental resolution. All 12 peaks correspond to distinct guided acoustic modes.

Brillouin spectra for the two sets of samples were recorded. Each spectrum consists of a series of discrete lines roughly symmetric about zero frequency shift. A typical spectrum from a sample grown on sapphire is shown in Fig. 1 and represents a 20-h integration. The contrast of $\cong 10^{10}$ for our interferometer is essential for the rejection of the intense elastically scattered light. The residual background in Fig. 1 is attributed primarily to the dark counts from the photomultiplier tube. Natural broadening of the observed lines, which correspond to guided modes, is insignificant compared to the instrumental broadening. The phase velocity for a surface guided wave is $V = \Omega/Q_p$, where Ω is the measured frequency shift and Q_p is the component of the acoustic wave vector parallel to the surface, determined from the scattering geometry. A least-squares fit of the instrumental transmission function is applied to each spectral line, and we obtain Ω from the average of the Stokes and anti-Stokes shifts. Measurements of reproducibility indicate that the uncertainty in Ω is $\cong 0.5\%$. Absolute velocity measurements have an added error of $\cong 1\%$.

The treatment by Farnell and Adler[13] of the acoustic modes in a supported film is the basis of our analysis. The substrate is treated as isotropic and the film as hexagonal, with the symmetry axis normal to the substrate. Only minor changes to the theory for an isotropic film are necessary to describe the transverse isotropy for such a film. The modes are still separable into Love modes, which are purely transverse and create no surface ripple, and the Rayleigh and Sezawa modes, which are polarized in the saggital plane and do ripple the surface. The Rayleigh wave is guided by the surface, while the Sezawa waves are freely propagating in the film and evanescent in the substrate. Of the five independent stiffness constants for the film, those which affect the Rayleigh and Sezawa phase velocities are c_{11}, c_{13}, c_{33}, and c_{44}. The remaining elastic constant c_{12} affects the dispersion of the Love modes. However, these are not detected in ripple-scattering measurements.

In principle, a single spectrum from one of the samples grown on sapphire has a sufficient number of modes to determine these four elastic constants. However, the dependences of c_{11}, c_{13}, and c_{33} on the mode velocities are nearly inseparable and thus a fit to the measured velocities is very sensitive to small errors. This causes $\cong 15\%$ variations among the fits to c_{11}, c_{13}, and c_{33} for different spectra when all four elastic constants are free parameters. By fixing c_{11} and c_{13} to their respective averages over the two separate data sets and allowing only c_{33} and c_{44} to freely vary during the least-squares fitting, variations in c_{33} were much reduced. We chose to free c_{33} because of an observed Λ-dependent strain normal to the film surface which we discuss below. It must therefore be recognized that small variations observed in c_{33} may actually be caused by variations in c_{11} or c_{13}. The elastic constants which give the best fit to the data are compared with the bulk-based estimates in Table I for a representative sample from each set. The stiffnesses obtained from such a fit to a single spectrum were used to generate the set of dispersion curves shown in Fig. 2. The departure of the measured velocities from those calculated from the fit are less than 0.5%. In addition to plotting the data used in making this fit, we include velocities obtained at four different Q_p values using the same sample. It is apparent that the observed dispersion is in good agreement with that predicted by the acoustic theory for a hexagonal film. The anisotropy of the film was verified by fitting the data to an isotropic model. These fits had Rayleigh velocities $\cong 1\%$ faster and Sezawa velocities $\cong 2\%$ slower than the measured velocities. The quality of the fit in Fig. 2 is representative of the entire set of spectra.

Ripple scattering is found to accurately account for the relative intensities of the peaks in our spectra. A general treatment of Brillouin scattering from thin-supported films[14] is the basis of a computer model we have used for calculating the scattering cross section. While the program can account for ripple- and elasto-optic scattering

TABLE I. The stiffnesses which provide the best fit to data from two samples are compared with the bulk-based estimates (the uncertainties indicate the span between the Voigt and Reuss estimates).

	Mo (vol%)	Λ(Å)	c_{11}	c_{12}	c_{13}	c_{33}	c_{44}
				(10^{10} N/m^2)			
Bulk			35.2(2)	15.9(1)	15.7(1)	34.1(2)	8.7(2)
fit	50	171	37.2	· · ·	14.9	34.0	8.15
Bulk			35.8(2)	16.0(1)	15.8(1)	34.6(2)	8.9(2)
fit	54	160	37.8	· · ·	15.0	33.2	7.86

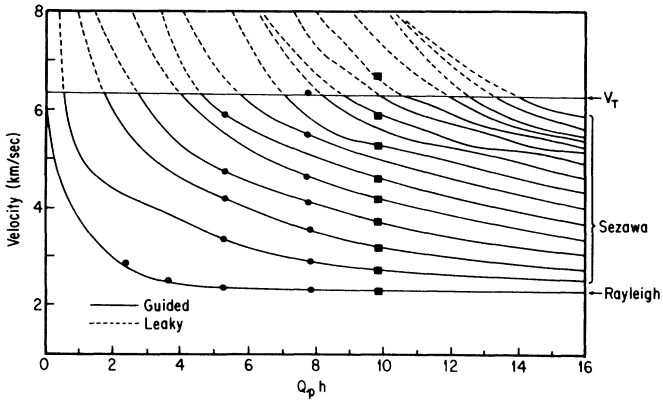

FIG. 2. Experimental velocities obtained at five different scattering angles for the sample used in Fig. 1. The solid curves are the best fit to the data obtained at $Q_p h = 9.83$ (squares). For velocities greater than the substrate shear velocity, the guided waves become leaky and couple to the bulk substrate waves. This fit is seen to accurately account for the experimental dispersion.

processes, we find that including only the ripple term leads to very good agreement with the measured spectra. The elastic constants obtained from the fit used to generate Fig. 2 were used as input to this program. Instrumental broadening is included by convolving the localized modes (originally Dirac δ functions) with a Gaussian distribution of matching width. Also, the absolute cross section has not been measured, so we have adjusted the intensity scale of the calculated spectrum such that the Rayleigh wave intensity is equal to the observed value. The comparison of this calculation with the data is shown in Fig. 3 and the agreement with the measured spectrum is excellent.

We find negligible differences among a series of spectra obtained by rotating a sample to different orientations about the normal axis. This supports our approximation that the sapphire substrate is isotropic.[15] The samples grown on isotropic fused silica were used as an added check of this approximation. Since there are fewer guided modes in these samples than in the films grown on sapphire, determination of the elastic constants is not as reliable. However, by fixing the values of c_{11} and c_{13} as described above, no significant differences in the fits to c_{33} and c_{44} for the different substrates are found.

Results of our analysis of the elastic constants for both sets of samples are plotted in Fig. 4. The error bars account for relative uncertainties attributed to measurements of film thickness and velocities. As seen in Fig. 2, the Rayleigh wave is quite insensitive to film thickness as long as the angle of incidence and scattering are large. A small uncertainty of 1% can be assigned to c_{44} since it is primarily determined by the Rayleigh wave velocity. The larger uncertainty of 4% for c_{33} is caused by an increased dependence on the Sezawa waves, which are very sensitive to film thickness. The error bars do not account for the $\cong$4% uncertainty in the film density. We have used the bulk density in our analysis. If this value is changed, nearly proportional changes must be made to all the elastic constants found from the fits. Additional errors in the absolute values of both c_{33} and c_{44} arising from uncertainties in the scattering geometry could be as large as 2%.

The observed variation of c_{44} vs Λ is found to be $\cong$10%. With one exception,[4] this is a much smaller variation than in all previous studies.[1-3] In the case of the Mo/Ni system,[2] a reduction in stiffness of $\cong$45% was reported to be associated with a concurrent 2.0% increase in the average lattice spacing $\bar{d}$ normal to the layers. Similar measurements of the average lattice spacing for our Mo/Ta superlattices[16] find only a 0.83% increase in $\bar{d}$ when varying Λ from 100–20 Å. This variation has been interpreted as a localized strain, normal to the layers, within $\pm$5 Å of the Mo/Ta interfaces.[16] The reduced variation in c_{44} reported here along with this smaller shift in $\bar{d}$ for the Mo/Ta sys-

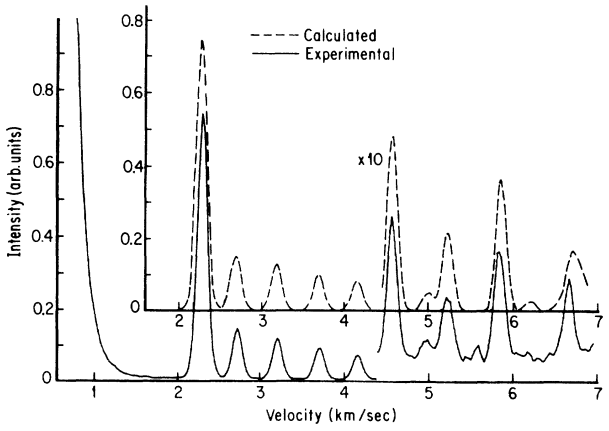

FIG. 3. Comparison of the light-scattering data as shown in Fig. 1 with the calculated intensity based on the elastic constants obtained from least-squares fitting the velocities of the surface waves. The theoretical results have been vertically offset to prevent the curves from overlapping.

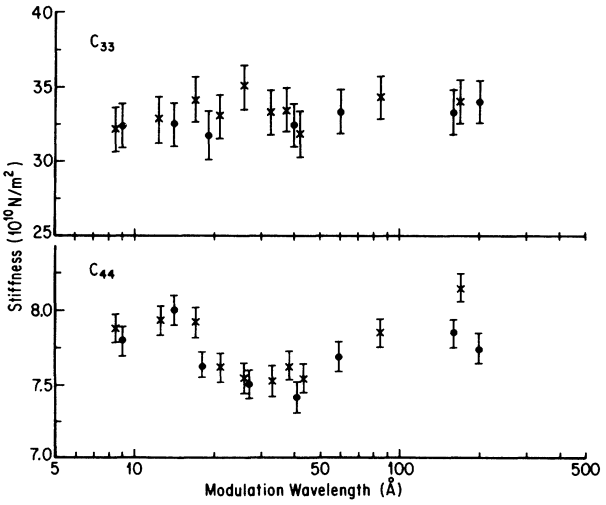

FIG. 4. Superlattice modulation wavelength dependence of the elastic constants determined by fitting the measured phase velocities to an acoustic model. Samples with 50% Mo are shown as crosses and 54% Mo as dots.

tem supports the association of these two separate properties. We believe that an additional property linked to these stiffness variations is the ratio R of the in-plane atomic densities for the two metals. From the bulk lattice constants for Mo/Ta, $R=1.11$ for the (110) planes. This is much closer to unity than for the Mo/Ni system where $R=1.31$ [this uses the (111) plane for Ni]. For Fe/Pd, another bcc-fcc system, the lattice mismatch at the interface is more like Mo/Ta with $R=0.89$ and no significant Λ dependence on the Rayleigh velocity was found.[4] With this experimental evidence, we feel that the interfacial lattice mismatch, the localized strain at the interface, and the Λ dependence of both $\bar{d}$ and c_{44} are all closely coupled.

We chose to look at changes in c_{33} (as opposed to c_{11} or c_{13}) because of the known variation in $\bar{d}$ which should affect the normal compressibility. As seen in Fig. 4, no significant changes in c_{33} were detected. This is quite different from the recent study of the Fe/Pd system[4] (which is the exception mentioned above), where a large softening of c_{11} is seen as the layer thickness decreases.

In conclusion, accurate measurements of the phase velocities of many distinct localized modes in Mo/Ta superlattices have been made. Close agreement with the calculated dispersion of these acoustic modes was found by treating the film as a homogeneous hexagonal solid. The bulk-based estimates of the stiffnesses c_{11}, c_{13}, c_{33}, and c_{44} all depart significantly from the values which best fit the data. A ripple-scattering theory for the relative cross section matches the Brillouin surface spectra quite precisely. By varying the bilayer wavelength of the samples, we find the magnitude of variations in the elastic constants c_{33} and c_{44} to be less than any other metal-metal superlattice yet studied by Brillouin scattering. Two possible causes for this relative uniformity are that the two metals have the same structure (i.e., bcc-bcc) and the lattice constants are closely matched. A slight softening of c_{44} occurs in the same range of bilayer wavelengths where the average lattice spacing increases. No significant variation in c_{11}, c_{13}, or c_{33} was detected.

We wish to acknowledge valuable assistance from J. Leavitt and J. Makous and helpful discussions with S. M. Lindsay, R. Mock, J. R. Sandercock, and B. Hillebrands. This work has been supported by the Joint Services Optics Program of the Army Research Office and Air Force Office of Scientific Research.

---

*Present address: Dipartimento di Fisica, Università di Modena, I-41100 Modena, Italy.

[1]A. Kueny, M. Grimsditch, K. Miyano, I. Banerjee, C. M. Falco, and I. K. Schuller, Phys. Rev. Lett. **48**, 166 (1982).

[2]M. R. Khan, C. S. L. Chun, G. P. Felcher, M. Grimsditch, A. Kueny, C. M. Falco, and I. K. Schuller, Phys. Rev. B **27**, 7186 (1983).

[3]R. Danner, R. P. Huebener, C. S. L. Chun, M. Grimsditch, and I. K. Schuller, Phys. Rev. B **33**, 3696 (1986).

[4]P. Baumgart, B. Hillebrands, R. Mock, G. Guntherodt, A. Boufelfel, and C. M. Falco, Phys. Rev. B **34**, 9004 (1986).

[5]A. Kueny, M. Grimsditch, B. Y. Jin, J. B. Ketterson, and J. B. Hilliard, J. Appl. Phys. **56**, 1550 (1984).

[6]R. Loudon, Phys. Rev. Lett. **40**, 581 (1978).

[7]B. A. Auld, *Acoustic Fields and Waves in Solids* (Wiley, New York, 1973), Vol. II, p. 97.

[8]C. M. Falco, W. R. Bennett, and A. Boufelfel, in *Dynamical Phenomena at Surfaces, Interfaces and Superlattices,* edited by F. Nizzoli, K. H. Rieder, and R. F. Willis (Springer-Verlag, Berlin, 1985), p. 35.

[9]J. M. Dickinson and P. E. Armstrong, J. Appl. Phys. **38**, 602 (1967); F. H. Featherston and J. R. Neighbours, Phys. Rev. **130**, 1324 (1963).

[10]M. J. P. Musgrave, *Crystal Acoustics* (Holden-Day, San Francisco, 1970), p. 177.

[11]M. Grimsditch, Phys. Rev. B **31**, 6818 (1985).

[12]S. M. Lindsay, M. W. Anderson, and J. R. Sandercock, Rev. Sci. Instrum. **52**, 1478 (1981); J. R. Sandercock, in *Light Scattering in Solids III,* edited by M. Cardona and G. Guntherodt (Springer-Verlag, Berlin, 1982), p. 173.

[13]G. W. Farnell and E. L. Adler, in *Physical Acoustics,* edited by W. P. Mason and R. N. Thurston (Academic, New York, 1972), Vol. 9, pp. 35–48.

[14]V. Bortolani, A. M. Marvin, F. Nizzoli, and G. Santoro, J. Phys. C **16**, 1757 (1983).

[15]The crystal orientation for the sapphire substrate is not completely specified. In making the isotropic approximation, we have set $c_{11}=49.7$ and $c_{44}=19.0$ N/m^2, which are the midpoints calculated from the allowed extrema of longitudinal and shear wave velocities, respectively. Changing these values to either extreme results in shifting the Sezawa velocities $<1\%$.

[16]W. R. Bennett, Ph.D. dissertation, University of Arizona, 1985 (unpublished); W. R. Bennett, J. A. Leavitt, and C. M. Falco, Phys. Rev. B (to be published).